Multiscale observations of CO_2, $^{13}CO_2$, and pollutants at Four Corners for emission verification and attribution

Rodica Lindenmaier[a,1], Manvendra K. Dubey[a,1], Bradley G. Henderson[b], Zachary T. Butterfield[a], Jay R. Herman[c], Thom Rahn[a], and Sang-Hyun Lee[a,2]

[a]Earth and Environmental Sciences and [b]Space and Remote Sensing, Los Alamos National Laboratory, Los Alamos, NM 87545; and [c]Goddard Space Flight Center, Joint Center for Earth Systems Technology, University of Maryland, Greenbelt, MD 20771

Edited* by Steven C. Wofsy, Harvard University, Cambridge, MA, and approved April 17, 2014 (received for review November 21, 2013)

There is a pressing need to verify air pollutant and greenhouse gas emissions from anthropogenic fossil energy sources to enforce current and future regulations. We demonstrate the feasibility of using simultaneous remote sensing observations of column abundances of CO_2, CO, and NO_2 to inform and verify emission inventories. We report, to our knowledge, the first ever simultaneous column enhancements in CO_2 (3–10 ppm) and NO_2 (1–3 Dobson Units), and evidence of $\delta^{13}CO_2$ depletion in an urban region with two large coal-fired power plants with distinct scrubbing technologies that have resulted in $\Delta NO_x/\Delta CO_2$ emission ratios that differ by a factor of two. Ground-based total atmospheric column trace gas abundances change synchronously and correlate well with simultaneous in situ point measurements during plume interceptions. Emission ratios of $\Delta NO_x/\Delta CO_2$ and $\Delta SO_2/\Delta CO_2$ derived from in situ atmospheric observations agree with those reported by in-stack monitors. Forward simulations using in-stack emissions agree with remote column CO_2 and NO_2 plume observations after fine scale adjustments. Both observed and simulated column $\Delta NO_2/\Delta CO_2$ ratios indicate that a large fraction (70–75%) of the region is polluted. We demonstrate that the column emission ratios of $\Delta NO_2/\Delta CO_2$ can resolve changes from day-to-day variation in sources with distinct emission factors (clean and dirty power plants, urban, and fires). We apportion these sources by using NO_2, SO_2, and CO as signatures. Our high-frequency remote sensing observations of CO_2 and coemitted pollutants offer promise for the verification of power plant emission factors and abatement technologies from ground and space.

air pollution | greenhouse gases | climate change

Trace gas [nitrogen oxides (NO_x), sulfur dioxide (SO_2), and carbon monoxide (CO)] and carbon dioxide (CO_2) emissions from anthropogenic fossil energy production are major contributors to air pollution and global warming. Under the Clean Air Act, in the United States these emissions are considered a threat to public health and welfare and are regulated by the Environmental Protection Agency (EPA). Although reporting requirements for air pollutants are well established, they are still under development for CO_2. Reported inventories of CO_2 and pollutant gases are calculated for specific activities using emission factors that depend on fuel composition, combustion efficiency, and scrubbing methods. These bottom–up inventories are subject to significant uncertainties and manipulations (1). Alternatively, atmospheric observations offer an independent top–down method to verify emissions of pollutant trace gases that have low atmospheric background levels and exhibit large and distinct increases near various combustion sources. For example, satellite observations of NO_2 have been used to evaluate regional and local emissions (2), but they are only useful for trend analysis, because their large observational footprint can underestimate NO_2. In contrast, background levels of CO_2 are high with significant variability, making source attribution and verification by direct CO_2 measurements elusive (3), limiting our ability to develop an effective global climate treaty or carbon-trading scheme (4). We postulate that measurements of coemitted trace gases and isotopic composition can be used to isolate anthropogenic CO_2 emissions and identify contributions from specific sectors with distinct composition (trace gas-to-CO_2 emission ratios, $ER_X = X/CO_2$, or isotopic ratio $^{13}CO_2/^{12}CO_2$). We hypothesize that remote column trace gas measurements over large scales, which are less sensitive to small-scale variability from meteorology than in situ point surface measurements, can provide a more precise method for identifying trends in emissions and emission factors (5). We evaluate this method by using extensive ground-based in situ and remote observations, and forward modeling using reported in-stack emissions at a site with large power plant emissions of CO_2 and pollutants.

Site and Instrumentation

Our monitoring site is located in Farmington, New Mexico (36.79°N 108.48°W, at 1,643 m above sea level), a semiarid region with two large coal-fired power plants that emit ~30 Mton/y of CO_2 and 80 Kton/y of NO_x (http://ampd.epa.gov/ampd/). The distance between the two power plants is nearly 13 km, making this region the largest point source of pollution in North and South America. The Four Corners power plant (FCPP) has high $\Delta NO_x/\Delta CO_2$ and is located ~12 km south of our site, whereas

Significance

Climate change and air pollution caused by fossil-energy-related CO_2 and NO_x emissions is a capstone societal issue. A critical barrier to an international treaty aimed toward controlling emissions is the inability to verify inventories and reduction of emissions claimed by individual nations following implementation of new technologies. We demonstrate for the first time, to our knowledge, that simultaneous remote observations of CO_2, NO_2, and CO regional column enhancements can be made with high fidelity and frequency. These can then be used to identify emissions from power plants and to distinguish them from other sources. Our findings represent a significant advancement in remote sensing monitoring methodology and can be used to develop an enforceable, transparent, and equitable climate treaty.

Author contributions: R.L. and M.K.D. designed research; R.L. and M.K.D. performed research; S.-H.L. contributed WRF-Chem modeling results; R.L., B.G.H., Z.T.B., J.R.H., and T.R. analyzed data; and R.L. and M.K.D. wrote the paper.

The authors declare no conflict of interest.

*This Direct Submission article had a prearranged editor.

Freely available online through the PNAS open access option.

[1]To whom correspondence may be addressed. E-mail: rodica@lanl.gov or dubey@lanl.gov.

[2]Present address: Department of Atmospheric Sciences, Kongju National University, Gongju 314-701, South Korea.

This article contains supporting information online at www.pnas.org/lookup/suppl/doi:10.1073/pnas.1321883111/-/DCSupplemental.

the San Juan power plant (SJPP) has low $\Delta NO_x/\Delta CO_2$ due to environmental upgrades and is 3.7 km east of our site (Fig. 1). Both power plants burn coal extracted from the San Juan Basin. The region also has dispersed urban emissions with much higher $\Delta NO_x/\Delta CO_2$ than the power plants emanating from Farmington and Bloomfield, located 10 and 30 km southeast of our site (Fig. 1). We analyze column CO_2, CO, and $^{13}CO_2$ retrieved from spectra recorded by a Bruker 125HR solar spectrometer (henceforth the 125HR) and column NO_2 retrieved from spectra recorded by a Pandora CCD solar spectrometer (Pan23, the 23rd such instrument worldwide), and compare these results with in situ measurements made using a Picarro G2401 analyzer (CO_2, CO), a Picarro G2101-i analyzer ($^{13}CO_2$), a Model 42*i* chemiluminescence nitrogen oxides analyzer (NO_2, NO_x), and a Model 43*i* pulsed UV fluorescence analyzer (SO_2). A description of these instruments and their precision and accuracy is given in *SI Text*. The 125HR was installed in March 2011 and operated continuously until November 2013, and is part of the Total Carbon Column Observing Network (TCCON; https://tccon-wiki.caltech.edu/; 6). The Pan23 column NO_2 measurements began in June 2012 and are ongoing.

Results and Discussion

We analyze measurements taken over a 4-month period from June 5, 2012 through the end of September 2012. Our analysis focuses on the plume composition measured by all instruments during clear-sky or partially cloudy conditions. We report, to our knowledge, the first simultaneous remote column observations of CO_2, CO, and NO_2 and evidence of $\delta^{13}CO_2$ depletion in the power plant plumes. The time series of column trace gas measurements are strongly correlated with in situ measurements recorded during plume events, demonstrating that column increases are indeed associated with local and regional pollution (Fig. 2). However, because in situ and remote sensors measure the gases at disparate spatial scales, some temporal shifts that can be attributed to meteorological conditions are exhibited. Specifically, we demonstrate that changes in weather patterns can cause variations in apparent source of CO_2 emissions that could not be attributed if not for distinct differences in the emission factors of the urban sources and each of the power plants. These differences allow us to distinguish column emission ratios of $\Delta NO_2/\Delta CO_2$ and identify the source of the emission. The phrase "emission ratio" will be used throughout the remainder of the text to refer to the ratio of the change in NO_2, NO_x, SO_2, and CO to the change in CO_2, where change (Δ) is considered to be any enhancement compared with the baseline that is observed during clean days.

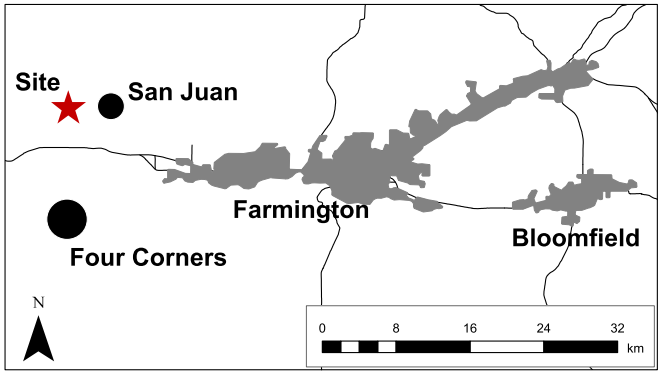

Fig. 1. Map showing the Four Corners region. The location of the site is marked by the red star, and the two power plants are marked by two full black circles. The magnitude of the circles indicates that the FCPP has an emission factor for $\Delta NO_2/\Delta CO_2$ double that of the SJPP. The urban region to the southeast is also shown.

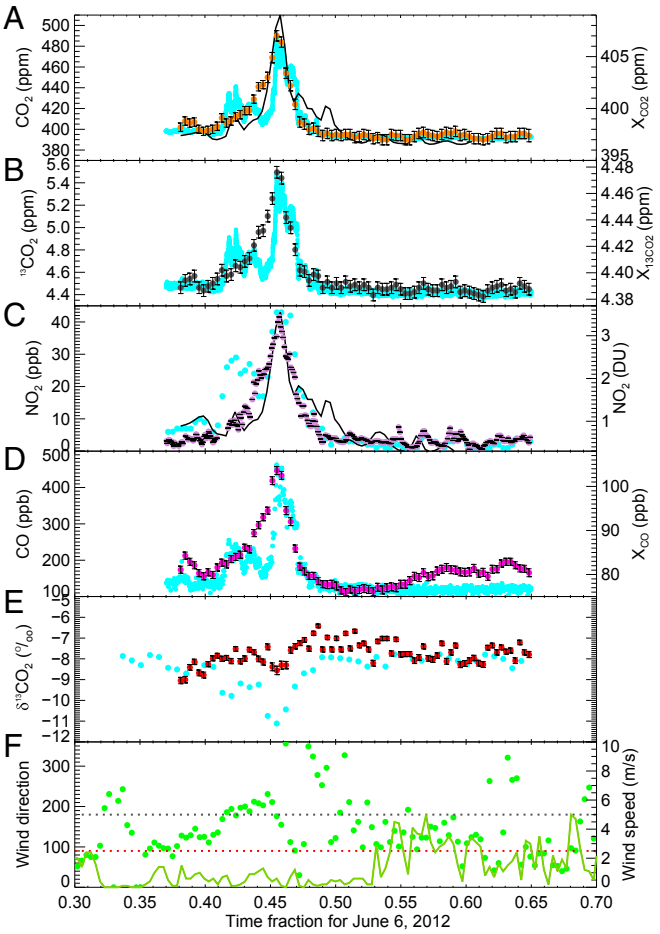

Fig. 2. Observed time evolution of CO_2, $^{13}CO_2$, NO_2, CO, and $\delta^{13}CO_2$ on June 6, 2012. (*A*, *B*, and *D*) 125HR column-averaged dry-air mole fractions of CO_2 (X_{CO2}, orange), $^{13}CO_2$ (X_{13CO2}, dark gray), and CO (X_{CO}, magenta), respectively, superimposed on the Picarro in situ values of the same gases (cyan). (*C*) Pandora (light purple) NO_2 total columns superimposed on the EPA in situ (cyan) NO_2 measurements. The black line in *A* and *C* is the simulated X_{CO2} and X_{NO2} by the nested WRF-Chem model, adjusted in space (0.6 km N) and time (+1 h). (*E*) $\delta^{13}CO_2$ (red) calculated from the 125HR measurements smoothed by the empirical function (Eq. **1**) and calculated from the Picarro in situ measurements (cyan). For clarity, error bars are indicated only for column results. For *A*–*D*, the primary *y* axis represents the in situ measurements, and the secondary *y* axis represents the column measurements. (*F*) Wind direction (green circles), where 0° corresponds to a wind from the north, and increasing clockwise (red and black dotted lines indicate 90° and 180°, respectively). The wind speed (solid green line) is reflected in the secondary *y* axis.

In Situ and Remote Column Measurements. Fig. 2 illustrates the in situ and regional columnar composition of the atmosphere and its time evolution on a typical day (June 6, 2012) when our instruments sampled the power plant plume. We observe an early morning column X_{CO2} (column-averaged dry-air mole fractions for CO_2; see *SI Text* for an in-depth explanation) of 398 ppm, 5 ppm higher than the clean air background measured on days when the wind blows from areas where fossil energy sources are nonexistent (the northwest). This increased morning signal indicates regional scale column CO_2 enhancements from the power plant emissions persisted due to overnight accumulation facilitated by meteorology. At 9:30 AM (time fraction 0.40), we see a clear rise in X_{CO2} that peaks at 407 ppm at 10:55 AM (time

ENVIRONMENTAL SCIENCES

fraction 0.45; Fig. 2*A*) and subsides by 11:30 AM (time fraction 0.48). The evolution of the other gases across time had similar patterns as the evolution of X_{CO2} (Fig. 2 *B*–*E*): X_{13CO2} increases by ∼0.1 ppm, NO_2 by 3.1 Dobson Units (DU), and X_{CO} by roughly 30 ppb. Fig. 2 also shows the in situ measurements of CO_2, $^{13}CO_2$, NO_2, and CO for June 6, indicating synchronous increases in all species that occurred between 9:00 AM (time fraction 0.38) and 12:00 PM (time fraction 0.50) local time. All of the in situ peaks are above the background level (CO_2 rose by 90 ppm, $^{13}CO_2$ by 1.1 ppm, NO_2 by 40 ppb, and CO by 370 ppb), and because the emissions are close to the surface, they are much larger than the column observations. The peaks in the in situ chemical and isotopic data demonstrate that our site intercepted the power plant and some urban plume during this period. This is verified independently by the observed meteorology. On June 6, 2012, the wind direction before the occurrence of the peaks was east and east–southeast (90–110°), bringing the SJPP and urban plumes to our site (Fig. 2*F*). The decrease in the trace gas concentrations that occurred after local noon coincided with winds that came from northern regions where there are no fossil energy combustion sources. Increased speed winds (>4 m/s) blowing from the southeast during the afternoon also resulted in smaller increases in the trace gas concentrations.

A tight correlation between in situ SO_2 and NO_x for the sampled air ($r = 0.99$) demonstrates that the power plants, sole emitters of SO_2, were the dominant sources of these gases at our site for this period (7, 8). We can verify the $\Delta NO_x/\Delta CO_2$ and $\Delta SO_2/\Delta CO_2$ emission ratios reported by in-stack monitors from our in situ atmospheric increases during the plume enhancements. These ratios are conserved as the power plant plume disperses into the atmosphere, because the lifetimes of the gases are longer than the transport times to our site. Hence, atmospheric measurements of these ratios can be used to verify the emission factors reported by in-stack power plant monitors (7, 8). The easterly winds indicate a plume from the SJPP, which is evident from the high correlations ($r > 0.95$) between NO_x, NO_2, SO_2, and CO_2 (Fig. S1*A*). We determine the in situ emission ratios of our plume observations for $\Delta NO_2/\Delta CO_2$ (5.3×10^{-4}), $\Delta NO_x/\Delta CO_2$ (1.5×10^{-3}), and $\Delta SO_2/\Delta CO_2$ (3.0×10^{-4}) by least-squares linear regression (9). $\Delta NO_x/\Delta CO_2$ and $\Delta SO_2/\Delta CO_2$ ratios are in strong agreement with the hourly emissions reported during the same time period by in-stack monitors at the SJPP (within 2.0% and 5.1%, respectively; Table S1). In comparison, these SJPP factors are approximately half of those reported by the FCPP, which is consistent with the deployment of upgraded NO_x and SO_2 scrubbers at SJPP starting in 2006 and completed in 2009 ($320 million environmental upgrade; www.pnm.com/systems/sj.htm). Likewise, there is good agreement between the estimated in situ $\Delta CO/\Delta CO_2$ emission ratio (3.7×10^{-3}) for June 6 (Fig. S1*B*) and values observed at other power plants (7, 8).

The regional column $\Delta NO_2/\Delta CO_2$ emission ratio was determined to be 3.7×10^{-4} for June 6 using the correlation plot (Fig. S2*A*) of the Pandora NO_2 and 125HR CO_2 columns, and is about 70% of the in situ value measured during the plume interception. A likely reason for this is that the column solar measurements sample a large region of the atmosphere (from surface to 100 km) and observe a spatial average of the air mass fractions over tens of km with polluted and clean air. Additional days with similar meteorological conditions (Figs. S3 and S4) also had constant column/in situ $\Delta NO_2/\Delta CO_2$ ratios of ∼70%. Similar results were achieved using CO, an independent pollutant tracer. The CO versus CO_2 correlation plot indicated a $\Delta CO/\Delta CO_2$ emission ratio of 2.8×10^{-3} (Fig S2*B*), and the $\Delta CO/\Delta CO_2$ column/in situ ratio was 76%. This agreement in the independently derived regional polluted air mass fractions indicates consistency among individual plumes (Table S1). The slightly lower value for $\Delta NO_2/\Delta CO_2$ compared with $\Delta CO/\Delta CO_2$ could be the result of the conversion of some NO_2 to HNO_3 at longer transit time and/or the presence of more distributed CO sources such as transport and fires.

High-resolution (200 m) simulations were also performed using a nested Weather Research Forecast–Chemistry (WRF-Chem) model that focused on Four Corners, for June 6, 2012 (*SI Text*). The model used the hourly in-stack emissions reports to update regional emissions inventory (National Emission Inventory 2002 and Vulcan). The plume rise in the model was parameterized and was 100–300 m, depending on the meteorology. Model simulations were able to reproduce the observed time evolution of CO_2 and the large 10 ppm increase (Fig. 2*A*) after small spatial (0.6 km) and temporal (1 h) adjustments of the plume. Such adjustments are consistent with limited power plant plume dispersion studies in chemical transport models (8). This indicates that the high-resolution WRF-Chem captured the large-scale dynamics and mixing of the plume into the regional atmosphere for CO_2, which is long-lived (Fig. 2*A*, solid black line). However, the small-scale plume mixing with the ambient air was sluggish in our simulations as this subgrid process is not well represented in WRF-Chem. Therefore, although NO_x ($NO + NO_2$) simulations were stronger, entrainment of ambient O_3, which converts emitted NO to NO_2, was needed to match the large point increases in NO_2 that we observed (as shown in Fig. 2*C* by a solid black line). The simulated $\Delta NO_2/\Delta CO_2$ ratio for June 6, 2012 was 4.1×10^{-4}, consistent with our observations of a large polluted regional column fraction. More detailed high-resolution power plant plume dispersion and chemistry model studies are needed to quantify their uncertainty.

The key finding from our analysis of multiple plumes was that the polluted fraction of the regional atmosphere was substantial, relatively constant for a particular meteorology and primarily due to emissions from the two large power plants (Table S1).

Isotopic $^{13}CO_2$ Signatures. Compared with ambient CO_2, coal is isotopically light in ^{13}C, which results in emissions from coal power plants with a distinct $^{13}CO_2$ signature (approximately –27‰) (10) that is much more depleted in ^{13}C than the background value of –8‰. This difference is clearly resolved by our high-precision in situ measurements of the plume. The in situ $\delta^{13}CO_2$ (*SI Text* and Fig. 2*E*) and CO_2 (Fig. 2*A*) coevolve as mirror images; the covariation in the CO_2 peak and $\delta^{13}CO_2$ minimum is indicative of emissions from a coal-fired power plant that burns coal that is lighter in ^{13}C. By using simple linear mixing, we find a decrease in the $\delta^{13}CO_2$ time series of ∼5.5‰, which corresponds to the maximum increase in CO_2 of about 90 ppm and is consistent with the change shown in Fig. 2*E*.

To infer the isotopic composition of the coal power plant plume source from our atmospheric observations, we show the Keeling plot (10) for in situ measurements of the plume on three different days (Fig. 3). The intercept, –26.0 ± 0.5‰ (±1σ), of the least-squares linear regression between $\delta^{13}CO_2$ and $1/^{12}CO_2$ yields the isotopic composition of the CO_2 from the local coal used in the power plant. This derived value strongly agrees with the –26.5 ± 0.3‰ measured isotopic composition of coal samples from the local San Juan Basin (11), and it demonstrates that as long as the coal or other fuel used by a power plant has a distinct isotopic signature, we can use high-precision in situ $\delta^{13}CO_2$ observations to verify its origin.

Looking at the remote column $\delta^{13}CO_2$ results on June 6, we note that the column CO_2 increased by ∼10 ppm, or 2.52% at its peak relative to the baseline. For this same time, $\delta^{13}CO_2$ retrieved from the column Fourier transform spectrometer (FTS) data led to a well-defined trough with a maximum at approximately −12‰. An independent evaluation using simple linear mixing and our in situ Keeling result indicates a column decrease of $\delta^{13}CO_2$ on June 6 of 0.65‰ [2.52% × (−26.0)], which should yield a column $\delta^{13}CO_2$ value of −8.65‰. This demonstrates that our retrieved FTS column value is unrealistically low and

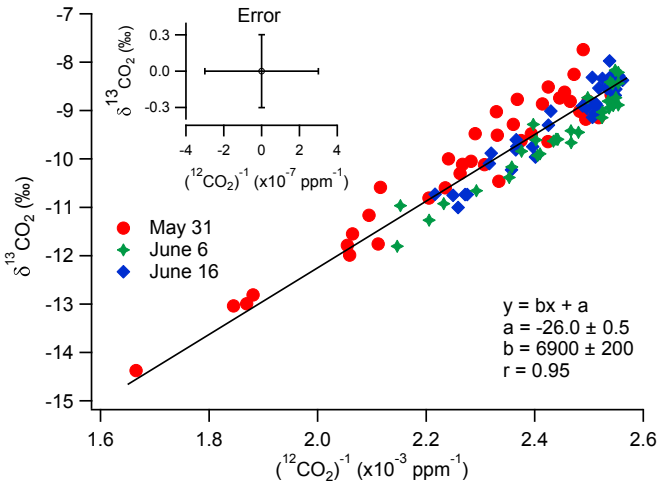

Fig. 3. Keeling plot for the in situ Picarro measurements on May 31 (red circles), June 6 (green stars), and June 16 (blue diamonds), 2012. The intercept, −26.0 ± 0.5‰, of the least-squares linear regression between the independent ($^{12}CO_2^{-1}$) and dependent ($\delta^{13}CO_2$) variables indicates the isotopic composition of the coal burned in the two power plants. The vertical error bar (±1σ) in the inset indicates the maximum error (0.3‰) for $\delta^{13}CO_2$, whereas the horizontal error bar shows the maximum error (3×10^{-7} ppm^{-1}) for $^{12}CO_2^{-1}$.

suggests that for our conditions the retrieved FTS column for $^{12}CO_2$ and $^{13}CO_2$ are not precise enough to yield $\delta^{13}CO_2$ estimates that are better than 3–4‰. In-depth analysis of the retrievals revealed that the most logical cause for the error is a combination of the difference in the averaging kernels for the two isotopologues and the significant atmospheric heterogeneity introduced by the plume. A comparison of the averaging kernels for this plume interception time period indicates that the two are definitely different. We conclude that in contrast to 0.6‰ claims in recent publications (12), current retrievals are unable to provide the fraction of per mil (‰) accuracy for $\delta^{13}CO_2$ in a heterogeneous atmosphere. The relatively low-noise dip seen in the measured $\delta^{13}CO_2$ signal indicates that our FTS spectra are indeed resolving (but not quantifying) the drop in $\delta^{13}CO_2$ created by the depleted plume, despite the fractional per mil estimated magnitude of −0.65‰. Therefore, to quantify the column $\delta^{13}CO_2$, we have adopted a semiempirical approach where we constrain the depletion at the peak to be −8.65‰, using our calibrated high-precision in situ measurements as a constraint as discussed earlier. We use an empirical function (Eq. **1**) to scale the "plume region" of $\delta^{13}CO_2$, where the $\delta^{13}CO_{2smooth}$ trough corresponds to −8.65‰:

$$\delta^{13}CO_{2smooth} = \delta^{13}CO_2 \times 0.15625 \times \left| ln\left\{ 0.0025 \times \left[1 + \left(\frac{CO_2^t - CO_2^{bkg}}{2.5} \right) \right] \right\} \right|, \quad [1]$$

where CO_2^t is the CO_2 value at time t and CO_2^{bkg} is the background CO_2 value (Fig. 2*E*). Comparable results were found for the plumes detected on May 31 (−8.91‰) and June 16 (−8.35‰; Figs. S3 and S4), indicating that our semiempirical column $\delta^{13}CO_2$ estimation methodology is robust and can be used to quantitatively retrieve column $\delta^{13}CO_2$ after it has been calibrated with in situ measurements at our site.

Source Attribution. We demonstrate that the column emission ratios of $\Delta NO_2/\Delta CO_2$ can resolve changes resulting from day-to-day variation in sources with distinct emission factors. We measured column CO_2 and NO_2 over a period of 117 days from June to September 2012, acquiring simultaneous observations of the two trace gases for 79 days. The over 3 ppm increase in X_{CO2} relative to the background on 69 of the days (87%) supports our claim that we sampled the regional emissions (i.e., power plant, urban, or fire) with high coverage. During this time frame we intercepted 123 plume events that lasted between 1 and several hours, some examples of which are featured in Fig. 4. The scatter-plots (least-squares linear regression) of column NO_2 versus column CO_2 are used to derive top–down emission factors ($\Delta NO_2/\Delta CO_2$) and to attribute the various sources. To help delineate the sources, we cluster these events into three groups based on the observed increases in NO_2 and CO_2 with examples in Fig. 4. The groups are classified as follows: group 1 (Fig. 4*A*) has large NO_2 but small CO_2 increases and represents 35.7% of all plume events, group 2 (Fig. 4*B*) has large increases for both NO_2 and CO_2 and dominates our dataset with 60.2% of all plume events, and group 3 (Fig. 4*C*) has small NO_2 but large CO_2 increases and accounts for the remaining 4.1% of the total number of plume events. The plumes analyzed in the first part of this work belong to group 2. There were also days when there were large shifts in the wind direction during the course of the day, resulting in multiple plume events that were a combination of groups 1 and 2 (e.g., Fig. S5). Finally, there were 8 clean days (10.1% of the total of 79 d) when the wind brought air from the northwest, where there are no emissions (e.g., June 10; Fig. 4*C*).

For events belonging to group 1, meteorological conditions indicate that winds emanated from the south and southeast, which brought air from the FCPP and the urban region (Fig. S6), but the signal subsided in the late afternoon due to southwesterly winds. The FCPP emits more CO_2 than the SJPP, but it is approximately three times farther (~12 km compared with ~3.7 km) from our site. The longer distance results in dilution of the FCPP plume as it mixes with the ambient air within the field of view of our solar spectrometer. However, this plume is mixed with polluted air with high $\Delta NO_2/\Delta CO_2$ from the urban region southeast of our monitoring site. The slopes of our column $\Delta NO_2/\Delta CO_2$ are the steepest for this group (5.17×10^{-4} to 14.0×10^{-4}; low cutoff value of 5×10^{-4}), partly because the FCPP has twice the $\Delta NO_2/\Delta CO_2$ emission factor of the SJPP, but mostly because urban emissions have much higher $\Delta NO_2/\Delta CO_2$ ratios than power plants (5×10^{-3}; 13). For group 1, the column/in situ ratios of $\Delta NO_2/\Delta CO_2$ (75%) are also larger compared with those belonging to group 2 (70%), with the exception of June 7 (65%; Table S1). This indicates that, for group 1, the measured column $\Delta NO_2/\Delta CO_2$ was high and that FCPP and urban sources contributed to the polluted regional air mass fraction. Moreover, the $\Delta CO/\Delta CO_2$ column/in situ ratios for this group exceed 90%, which were again larger than those observed for group 2 and consistent with a large urban contribution to the polluted regional air mass.

Meteorological conditions contribute to the complex day-to-day variability of the results, making their relationship intricate and necessitating the use of meteorological and other corroborative information for interpretation. Because SO_2 lifetime is on the order of days, we use the measured in situ $\Delta SO_2/\Delta CO_2$ emission ratio as a unique tracer for power plant emissions. For group 1, where the winds indicate air masses originating from the FCPP and the urban region, we can calculate the fraction of air sampled from each source by considering the FCPP emission value weighted by the in situ $\Delta SO_2/\Delta CO_2$ to FCPP $\Delta SO_2/\Delta CO_2$ ratios (Table S1). For example, on September 26, we found that 69% of the pollution came from the FCPP and 31% from urban sources (using a $\Delta NO_X/\Delta CO_2$ value of ~5×10^{-3} for urban emissions and in-stack data for FCPP).

Group 2 events are characterized by winds blowing from the east bringing air from the nearby SJPP and then changing to the east–southeast bringing some air from the urban region (Fig. S7). These meteorological conditions occurred on more than 60% of

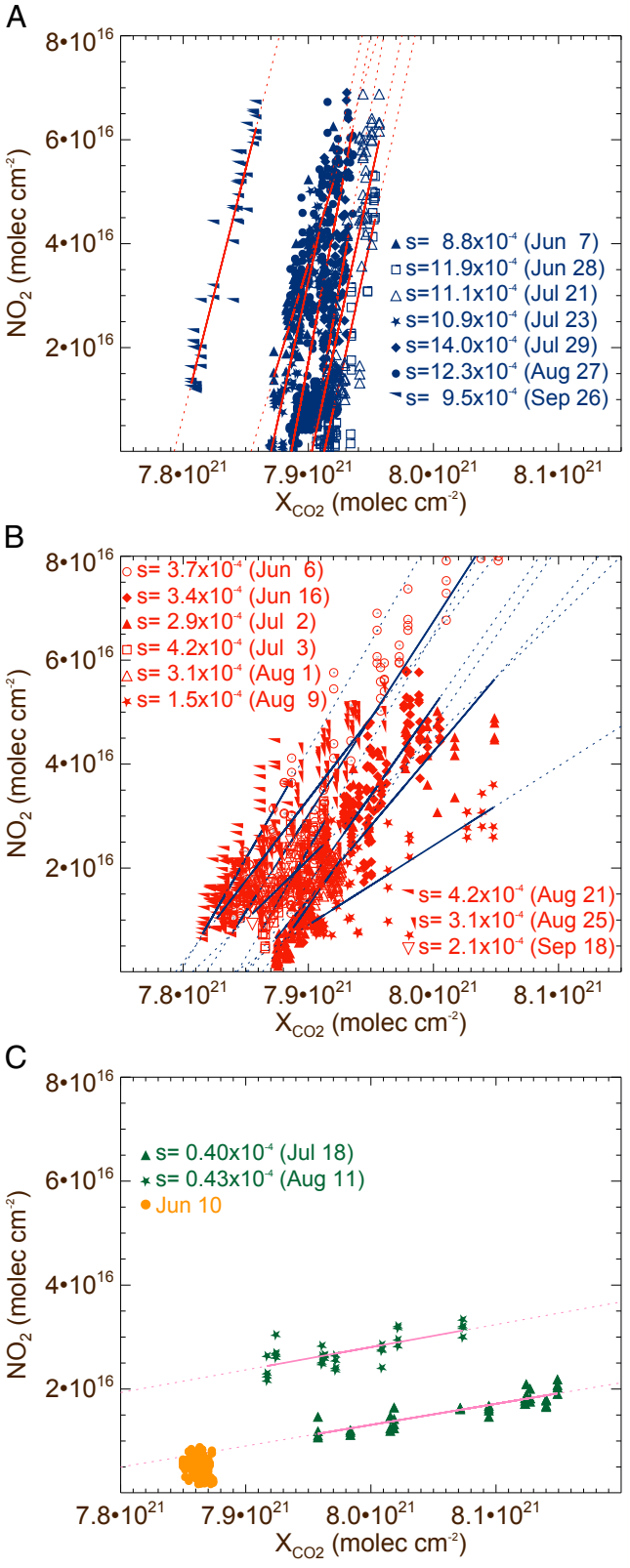

Fig. 4. Correlation plots for regional column NO_2 versus column CO_2 for selected plume events (19 of 123). Samples were collected between June 5 and September 30, 2012, and used to illustrate our ability to discriminate sources. Examples are shown for (*A*) group 1 (dark blue), cutoff slope value 5×10^{-4}; (*B*) group 2 (red), cutoff slope value 1×10^{-4}; and (*C*) group 3 (dark green), slope $<1 \times 10^{-4}$, and for a day without pollution (orange). Each group corresponds to sources with distinct emission factors and location relative to our site as discussed in the text.

the sampled days. Note that due to the proximity of our site to the SJPP, there was less dilution by mixing with ambient air, causing the NO_2 and CO_2 concentrations to be larger for group 2 than for group 1. Compared with group 1, there was much less mixing of the SJPP plume with urban pollution. For group 2, we determine the column $\Delta NO_2/\Delta CO_2$ ratio to be 2–10 times smaller (1.30×10^{-4} to 4.90×10^{-4}; low and high cutoff values of 1.0×10^{-4} and 5.0×10^{-4}, respectively) than for group 1, which is consistent with the smaller $\Delta NO_2/\Delta CO_2$ emission factor of the SJPP and the less intrusive mixing of the urban plumes for this meteorology. Our key finding is that our remote column measurements can resolve the emission factor differences from the FCPP plume, the SJPP plume, and the urban plume and are consistent with meteorology. Following the same rationale of using SO_2 as a marker for power plants as we did for group 1, we find that for May 31, 100% of the pollution is due to the SJPP, whereas for June 6, 98% is due to the SJPP and 2% from urban pollution. This is consistent with our site's proximity to the SJPP and the favorable wind patterns for sampling it relative to the urban plume.

Of particular interest are those days with mixed meteorological conditions, which are characterized by two plumes with different slopes. Our observations show that morning plumes usually belong to group 2, when winds mostly blow from the east, whereas afternoon plumes belong to group 1, when winds blow from the south–southeast. July 23 exemplifies this pattern (Fig. S5). First, the group 2 plume formed before local noon on this day (slope = 3.56×10^{-4}), followed by a second group 1 plume that formed after 1:30 PM (slope = 10.9×10^{-4}).

Group 3 events (Fig. 4*C*) can arise from nonfossil combustion sources that have lower $\Delta NO_x/\Delta CO_2$ emission ratios, such as fires, which have a slope $<1 \times 10^{-4}$. Furthermore, we find that group 3 has the highest in situ $\Delta CO/\Delta CO_2$ value of about 0.01 for all sampled days. The FTS X_{CO} column is also enhanced and correlates very well with X_{CO2} (e.g., on August 11, $r = 0.97$; Fig. S8*B*), having a high emission ratio value (5.2×10^{-3} for August 11). The high $\Delta CO/\Delta CO_2$ is due to incomplete combustion that is common in fires. Both observations suggest that we likely sampled air masses containing biomass-burning plumes. The $\Delta CO/\Delta CO_2$ column/in situ ratio for August 11 is 53 ± 5%, indicating a less polluted regional air mass fraction with CO originating from more remote regions, compared with groups 1 and 2. This finding was supported by the northwesterly wind direction observed on August 11 (Fig. S8*A*); these winds emanated from a region where there are no fossil energy sources. We examined the moderate resolution imaging spectroradiometer (MODIS) active fire detection archive during this period, which indicated massive wildfires in Nevada and Utah during the second week of August. Similarly, July 18 also had large enhancements of both X_{CO2} and X_{CO} (Fig. S8 *C* and *D*), indicating the presence of biomass burning emissions. Analysis of group 3 demonstrates our ability to identify and separate CO_2 emissions from fires using high $\Delta CO/\Delta CO_2$ as a proxy.

Our analysis of extensive and intensive chemical composition observations at multiple scales demonstrates that remote sensing of regional column NO_2, CO, and CO_2 is a powerful method to discriminate and attribute contributions of distinct sources with different emission factors quantitatively. The remote column $\Delta NO_2/\Delta CO_2$ ratios of FCPP and urban plume emission (group 1) are 2–10 times larger than those dominated by the SJPP emissions mixed with some urban plumes (group 2), yet the SJPP and urban plumes are 3–10 times larger than those from biomass burning (group 3). Atmospheric observations of other source-specific tracers (e.g., CH_2O, CH_3CN, or HCN for fires and hydrochlorofluorocarbons from vehicle air conditioners) can further improve our ability to delineate contributions of multiple sources to regional greenhouse gas and pollutant increases.

The world coal reserves are estimated to be 930 Gt, which suggests that the number of coal-fired power plants will continue

to expand, resulting in significant growth of CO_2 emissions (e.g., in China and India). The Kyoto protocol (http://unfccc.int/resource/docs/convkp/kpeng.pdf) requires the regular reporting of CO_2 emissions, but current reporting in non-US countries is based on bottom–up estimates that use the type of fuel burned, power plant thermal efficiency, and CO_2 conversion factors, rather than direct measurements of CO_2 emissions. Independent approaches are required to verify CO_2 emissions of individual power plants. The National Research Council recommends (14) the evaluation of satellites for this purpose and the ongoing Greenhouse Gases Observing Satellite, imminent Orbiting Carbon Observatory (OCO)-2, and the future CarbonSat mission should provide data to assess this (*SI Text*). Our high-frequency and precision ground-based remote-sensing results provide the performance metric and sampling strategy for satellite-based measurements, permitting a global emission monitoring system. We show that continuous high-frequency measurements from future geostationary satellites such as geoCARB have distinct advantages over single snapshot orbiting satellites for verification (15). Furthermore, our results show that simultaneous observations on NO_2, CO_2, CO, and SO_2 from the satellites have the potential to attribute various CO_2 sources and also verify power plant environmental technology upgrades to improve air quality.

Conclusions

We report simultaneous in situ and column remote measurements of anthropogenic plume composition in ambient air in a semiarid region with substantial emissions from two large coal-fired power plants in an urban setting. Our multiscale observations of trace gases and CO_2 capture the temporal evolution of the power plant plume composition with high fidelity. Our ground-based remote measurements of regional column $\Delta NO_2/\Delta CO_2$ ratios are compared with in situ plume ratios to show that a large and stable fraction of the regional atmosphere is polluted (70–75%) in the vicinity of large combustion sources. Regional-scale remote column observations average over the fine-scale variability in point measurements, providing a less noisy and smoothed observable for emission verification (5). The agreement between our column CO_2 and NO_2 plume observations and our forward model simulations with in-stack emissions suggests that the methodology could be used for verification. We demonstrate that our remote column $\Delta NO_2/\Delta CO_2$ observations can resolve large variations from regional sources with distinct emission factors and apportion them using other signatures such as SO_2 and CO. Our findings offer promise for future satellite-based monitoring approaches that simultaneously measure column CO_2 and NO_2 and determine emission factors from space. Long-term observations of atmospheric $\Delta NO_2/\Delta CO_2$ above power plants could allow for verification of $\Delta NO_2/\Delta CO_2$ emission factor reductions from technology improvement and provide reliable constraints to estimate reported CO_2 emissions (e.g., Vulcan; 16).

Materials and Methods

Observations. We focus on CO_2, NO_2, NO_x, SO_2, and CO and use in situ and ground-based remote column measurements for our study. In situ (point) measurements of CO, CO_2, and its isotopes were made using two Picarro gas analyzers. These analyzers have excellent stability and are based on the Wavelength-Scanned Cavity Ring-Down Spectroscopy technique (*SI Text*). NO_2 and NO_x were obtained from a chemiluminescence NO-NO_2-NO_x analyzer (*SI Text*), whereas SO_2 was obtained from a pulsed fluorescence analyzer (*SI Text*). All in situ instruments have a time resolution better than a minute. For column CO_2, $^{13}CO_2$, and CO measurements, a Bruker 125HR FTS was used. This instrument is part of the TCCON network and is designed for highly precise solar measurements in the near-infrared (NIR) spectral region (*SI Text*), with a high time resolution of ~3 min. NO_2 columns were derived from the Pandora CCD solar spectrometer (*SI Text*), which measured side-by-side with the 125HR. Our Pandora has a high time resolution of 20 s. Measurements from June 5 to September 30 were analyzed, of which typical examples are highlighted in this work. In situ and remote column emission ratios of $\Delta NO_2/\Delta CO_2$, $\Delta NO_x/\Delta CO_2$, $\Delta SO_2/\Delta CO_2$, and $\Delta CO/\Delta CO_2$ were used to resolve changes resulting from variations in the contributions from the two power plants, urban sources, and remote fires, all of which have distinct emission factors. Meteorology (from an onsite ZENO weather station, www.coastalenvironmental.com/) was used for the interpretation of the results and attribution to the correct source. Our observations were compared with real-time in-stack power plant emission values reported by the EPA (http://ampd.epa.gov/ampd/) for emission verification.

WRF-Chem Model. The WRF-Chem model Version 3.1 is used to simulate the chemical and physical behaviors of stack plumes over the complex terrain of our site. It is a 3D, fully compressible, nonhydrostatic meteorological model configured with five domains using a one-way nested large-eddy simulation approach. The inner nested domains are sequentially zoomed in on the Four Corners region with a nesting ratio of 3, with the finest domain encompassing the SJPP, FCPP, and our site resolved at 200 m. Anthropogenic emissions are prepared based on the US EPA's national emission inventory year 2005 for primary pollutants and the Vulcan gridded emissions for CO_2 (16), in which the anthropogenic emissions from the SJPP and FCPP were replaced by real-time Continuous Emissions Monitoring System-reported emissions for specific simulation days. Please refer to *SI Text* for further details on the modeling framework.

ACKNOWLEDGMENTS. We thank TCCON (D. Wunch and P. Wennberg) for providing resources to achieve high-accuracy retrievals. We thank A. Cede and N. Abuhassan for their continuous effort to optimize and maintain the Pandora instrument. We acknowledge the New Mexico Environment Department (T. Hertel, M. Jones, and R. Szkoda), EPA (M. Sather), and Bureau of Land and Management (M. Uhl) for providing us access to the site and in situ air quality data. S.-H.L. thanks the Korean Meteorological Administration for support with supercomputing resources. We thank R. Middleton and J. Muss [Los Alamos National Laboratory (LANL)] for editorial assistance. The reported research was supported by the LANL Laboratory Directed Research and Development project "Multi-Scale Science Framework for Climate Treaty Verification: Attributing & Tracking GHG Fluxes Using Co-Emitted Signatures" (principal investigator M.K.D.).

1. Guan D, Liu Z, Geng Y, Lindner S, Hubacek K (2012) The gigatonne gap in China's carbon dioxide inventories. *Nature Climate Change* 2(1560):672–675.
2. Richter A, Burrows JP, Nüss H, Granier C, Niemeier U (2005) Increase in tropospheric nitrogen dioxide over China observed from space. *Nature* 437(7055):129–132.
3. Marquis M, Tans P (2008) Climate change. Carbon crucible. *Science* 320(5875): 460–461.
4. Committee on Methods for Estimating Greenhouse Gas Emissions (2010) *Verifying Greenhouse Gas Emissions: Methods to Support International Climate Agreements* (National Research Council. National Academies Press, Washington, DC).
5. McKain K, et al. (2012) Assessment of ground-based atmospheric observations for verification of greenhouse gas emissions from an urban region. *Proc Natl Acad Sci USA* 109(22):8423–8428.
6. Wunch D, et al. (2011) The Total Carbon Column Observing Network. *Phil Trans R Soc A* 369(1943):2087–2012.
7. Peischl J, et al. (2010) A top-down analysis of emissions from selected Texas power plants during TexAQS 2000 and 2006. *J Geophys Res* 115:D16303.
8. Zhou W (2012) Observation and modeling of the evolution of Texas power plant plumes. *Atmos Chem Phys* 12(1):10.5194/acp-12-455-2012.
9. York D (1966) Least-squares fitting of a straight line. *Canadian Journal of Physics* 44(5):1079–1086.
10. Keeling CD (2001) *Exchanges of Atmospheric CO2 and 13CO2 with the Terrestrial Biosphere and Oceans from 1978 to 2000. I. Global Aspects*, SIO Reference Series, No. 01-06 (Scripps Institution of Oceanography, San Diego, CA).
11. Formolo M, Martini A, Petsch S (2008) Biodegradation of sedimentary organic matter associated with coalbed methane in the Powder River and San Juan Basins, U. S. A. *Int J Coal Geol* 76(1-2):86–97.
12. Reuter M, et al. (2012) On the potential of the 2041-2047 nm spectral region for remote sensing of atmospheric CO_2 isotopologues. *J Quant Spectrosc Radiat Transf* 113(16):2009–2017.
13. Kolb CE, et al. (2004) Mobile laboratory with rapid response instruments for real-time measurements of urban and regional trace gas and particulate distributions and emission source characteristics. *Environ Sci Technol* 38(21):5694–5703.
14. National Research Council (NRC)–Committee on Methods for Estimating Greenhouse Gas Emissions (2010) *Verifying Greenhouse Gas Emissions: Methods to Support International Climate Agreements*. Available at www.nap.edu/catalog/12883.html.
15. Rayner PJ, Utembe SR, Crowell S (2013) Constraining regional greenhouse gas emissions using geostationary concentration measurements: A theoretical study. *Atmos Meas Tech Discuss* 7(2):1367–1392.
16. Gurney KR, et al. (2009) The Vulcan Project: High resolution fossil fuel combustion CO_2 emissions flux for the United States. *Environ Sci Technol* 43(14):10.1021/es900806c.